

Large-eddy simulation using a discontinuous Galerkin spectral element method

K. Sengupta, * and F. Mashayek †

University of Illinois at Chicago

G.B. Jacobs, ‡

San Diego State University

In this paper we discuss the development of a robust, high-order discontinuous Galerkin (DG) spectral element method for large-eddy simulation (LES) of compressible flows. The method secures geometrical flexibility through a fully unstructured grid (triangles in 2D and tetrahedral elements in 3D), allows for arbitrary order of accuracy and has excellent stability properties. An element based filtering technique is used in conjunction with the dynamic procedure to model the effect of sub-grid scales. We aim to use the LES methodology for large-scale simulation in geometrically complex dump combustors. As a first step towards these simulations, we perform validation simulations of compressible, turbulent flow in a plane channel with isothermal walls.

Nomenclature

\bar{A}	Filtering
\tilde{A}	Favre filtered quantities
C_f	Skin friction coefficient
C_p	Specific heat capacity at constant pressure
C_v	Specific heat capacity at constant volume
C_s	Smagorinsky coefficient
c_{air}	Speed of sound in air
e	Total energy per unit mass
k	Thermal conductivity
L_f	Reference length
L_α	Lagrange interpolating polynomial
l_k	Filter coefficients
Ma	Mach number
M_f	Reference Mach number
\widehat{M}	Element mass matrix
N	Number of nodes in each element
\mathbf{n}	Normal vector
n	Polynomial order
Pr	Prandtl Number
Pr_t	Turbulent Prandtl number
p	Thermodynamic pressure

*Graduate student, Department of Mechanical and Industrial Engineering, 842 W. Taylor Street, Chicago, IL 60607.

†Professor, Department of Mechanical and Industrial Engineering, 842 W. Taylor Street, Chicago, IL 60607, AIAA Associate Fellow.

‡Assistant Professor, Department of Aerospace Engineering, 5500 Campanile Drive, San Diego, CA 92182

q_j	Heat flux vector
Re	Reynolds number
S_{ij}	Rate of strain tensor
\hat{S}	Element stiffness matrix
T	Temperature
U	Mean streamwise velocity
U^+	Friction velocity
U_{rms}	Streamwise RMS velocity
U_f	Reference velocity
u_i	Velocity vector
\mathbf{V}	Vandermonde matrix
V_{rms}	Normal RMS velocity

Greek

δ_{ij}	Kronecker delta
λ	Eigenvalue
ρ	Density
μ	Viscosity
σ_{ij}	Viscous stress tensor
γ	C_p/C_v

Subscript

f	Reference values
i	Coordinate direction
j	Coordinate direction
α	Matrix\vector index
β	Matrix\vector index

Superscript

T	Transpose
sgs	Subgrid scale quantities

I. Introduction

Large-eddy simulation (LES) is a suitable technique for simulating a large class of complex flows (unsteady flows, flows with large scale coherent structures, mixing and aero-acoustics). Under such circumstances they are preferred over direct numerical simulation (DNS) and Reynolds-averaged Navier-Stokes (RANS) methods. DNS involves accurate solution of time dependent governing equations without any modeling. It is capable of resolving all the temporal and spatial scales present in the flow and is therefore the ideal method for analyzing the flow dynamics. However, huge computational expense of DNS makes it unsuitable for practical flows. In RANS, on the other hand no attempt is made to resolve any of the turbulent motion, rather the net effect of all the scales on the mean flow is modeled. RANS methods, though computationally efficient are inadequate at capturing the true dynamics of the flow. They are generally used for predicting engineering parameters like lift, drag, and characteristic frequencies for design. LES is based on the concept of scale separation in turbulent flows: the large scales, which are anisotropic and sensitive to boundary conditions are computed directly as in DNS, while the small scales that are more isotropic and universal are modeled. They are superior to the RANS techniques at providing insight into the underlying physics. Moreover much lower computational cost compared to DNS, makes them a suitable candidate for application to practical flow studies.

Current high-order LES works rely mostly on spectral or compact finite difference^{1,2} methods on structured grids. While these methods have proven to be quite successful in providing insight into the physics of turbulence in simple configurations, their limitations show up in practical flows that deal with arbitrarily complex geometry. Dependence on structured grids limits geometric flexibility. Spectral methods guarantee higher accuracy but impose severe restrictions on boundary conditions by requiring a periodic computational domain. There have been attempts to resolve this issue by developing methods on unstructured grids. The

bulk of these techniques are based on finite element (e.g. Jansen³) or finite volume (e.g. Bui⁴) framework, that employ low-order spatial approximations. Large truncation and aliasing errors of these schemes lead to significant errors in the LES results.⁶

Spectral element methods offer several attractive features that make them excellent candidates for LES in complex geometries. They have previously been successfully applied to direct numerical simulation of turbulent flows.⁵ As higher-order finite element methods they can deal with arbitrary complex geometry. Moreover spatial resolution can be conveniently altered either by increasing the number of elements (h-refinement) or increasing the polynomial order within the elements (p-refinement). In smooth solution spaces, the methods provide asymptotically exponential rate of spatial convergence with p-refinement. LES within spectral element framework has started to gain attention only recently. Spectral element filtering strategies for LES has been studied by Blackburn and Schmidt⁷ and Levin et. al.⁸ Karamanos used an unstructured spectral/ hp finite element method⁹ for large eddy simulation using classical sub-grid models and more recently multidomain method¹⁰ to implement spectral vanishing viscosity concepts. The unstructured method used by Karamanos employs 2-dimensional spectral elements (triangles) and Fourier expansion in the third direction. To the best of the authors' knowledge there has been no previous attempt to develop spectral element LES code employing fully unstructured mesh.

In this paper, we present a high-order discontinuous Galerkin method on tetrahedral elements which addresses the restrictions of the lower order methods and structured grids. We combine an element-based filtering technique with dynamic estimation of the sub-grid constants to model the effect of unresolved scales.

The paper is organized as follows. First we describe the the governing equations for LES of compressible flows. Then we outline the numerical method used to solve the governing equations. Next we provide description of the sub-grid model together with the element based filtering technique used for its implementation. Finally, we present results for a 2D plane Poiseuille flow at high Reynolds number.

II. Governing Equations

A. Compressible Navier-Stokes

The governing equations for the compressible and viscous fluid flow are the conservation statements for mass, momentum and energy. They are presented in non-dimensional, conservative form with Cartesian tensor notation,

$$\frac{\partial \rho}{\partial t} + \frac{\partial(\rho u_j)}{\partial x_j} = 0, \quad (1)$$

$$\frac{\partial(\rho u_i)}{\partial t} + \frac{\partial(\rho u_i u_j + p \delta_{ij})}{\partial x_j} = \frac{\partial \sigma_{ij}}{\partial x_j}, \quad (2)$$

$$\frac{\partial(\rho e)}{\partial t} + \frac{\partial[(\rho e + p)u_j]}{\partial x_j} = -\frac{\partial q_j}{\partial x_j} + \frac{\partial(\sigma_{ij} u_i)}{\partial x_j}. \quad (3)$$

The total energy, viscous stress tensor and heat flux vector are given as,

$$\rho e = \frac{p}{\gamma - 1} + \frac{1}{2} \rho u_k u_k, \quad (4)$$

$$\sigma_{ij} = \frac{\mu}{Re} \left(\frac{\partial u_i}{\partial x_j} + \frac{\partial u_j}{\partial x_i} - \frac{2}{3} \frac{\partial u_k}{\partial x_k} \delta_{ij} \right), \quad (5)$$

$$q_j = -\frac{\mu}{(\gamma - 1) Re Pr M_f^2} \frac{\partial T}{\partial x_j}. \quad (6)$$

The Reynolds number Re is based on the reference density ρ_f^* , velocity U_f^* , length L_f^* , and molecular viscosity μ_f^* and is given by $Re = \rho_f^* U_f^* L_f^* / \mu_f^*$. $Pr = \mu_f^* C_p / k^*$ is the Prandtl number. The non-dimensional viscosity is taken as $\mu = \mu(T) / \mu_f^*$, where $\mu(T)$ is the molecular viscosity at temperature T . The superscript $*$ denotes dimensional quantities. The above equation set is closed by the equation of state,

$$p = \frac{\rho T}{\gamma M_f^2}, \quad (7)$$

where M_f is the reference Mach number, taken to be 1 in this work.

The conservation equations can be cast in the matrix form

$$\frac{\partial \mathbf{Q}}{\partial t} + \frac{\partial \mathbf{F}_i^a}{\partial x_i} - \frac{\partial \mathbf{F}_i^v}{\partial x_i} = 0, \quad (8)$$

where

$$\mathbf{Q} = \begin{pmatrix} \rho \\ \rho u_1 \\ \rho u_2 \\ \rho u_3 \\ \rho e \end{pmatrix}, \quad (9)$$

$$\mathbf{F}_i^a = \begin{pmatrix} \rho u_i \\ \rho u_1 u_i + p \delta_{i1} \\ \rho u_2 u_i + p \delta_{i2} \\ \rho u_3 u_i + p \delta_{i3} \\ (\rho e + p) u_i \end{pmatrix}, \quad (10)$$

$$\mathbf{F}_i^v = \begin{pmatrix} 0 \\ \sigma_{i1} \\ \sigma_{i2} \\ \sigma_{i3} \\ -q_i + u_k \sigma_{ik} \end{pmatrix}. \quad (11)$$

Here \mathbf{Q} is the vector of the conserved variables and will also be referred to as the state vector in this work. \mathbf{F}_i^a and \mathbf{F}_i^v are the advective and viscous flux vectors respectively, in the x_i direction.

B. Filtered Navier-Stokes

The main issue in LES is the separation of small scales or high frequency modes (in space) in order to reduce the number of degrees of freedom of the dynamical system and therefore make the problem more tractable. Thus, it is necessary to devise a mathematical model which would enable that. The most popular method is to apply a spatial low-pass (in frequency domain) convolution filter to the mathematical model which describes the flow exactly (i.e. Navier-Stokes equations). Alternate mathematical models have also been proposed (see Sagaut¹⁴ for details). Filtering in physical space is represented as a convolution product,

$$\bar{f}(\mathbf{x}, t) = \int_{\Omega} f(\mathbf{x}', t) G(\mathbf{x} - \mathbf{x}') d\mathbf{x}', \quad (12)$$

where G is the filter kernel and Ω represents the flow domain. For compressible flows it is convenient to apply density weighted filtering operation introduced by Favre.¹⁵ In Favre filtering, the filtered quantities are obtained as,

$$\tilde{f} = \frac{\bar{\rho f}}{\bar{\rho}}, \quad (13)$$

where overbar denotes the filtering operation. The above procedure leads to the following filtered conservation equations (assuming filtering commutes with differentiation),

$$\frac{\partial \bar{\rho}}{\partial t} + \frac{\partial (\bar{\rho} \tilde{u}_j)}{\partial x_j} = 0, \quad (14)$$

$$\frac{\partial (\bar{\rho} \tilde{u}_i)}{\partial t} + \frac{\partial (\bar{\rho} \tilde{u}_i \tilde{u}_j + \bar{p} \delta_{ij})}{\partial x_j} = \frac{\partial \tilde{\sigma}_{ij}}{\partial x_j} - \frac{\partial \tau_{ij}^{sgs}}{\partial x_j} + \frac{\partial (\bar{\sigma}_{ij} - \tilde{\sigma}_{ij})}{\partial x_j}, \quad (15)$$

$$\frac{\partial(\bar{\rho e})}{\partial t} + \frac{\partial[(\bar{\rho e} + \bar{p})\tilde{u}_j]}{\partial x_j} = -\frac{\partial\tilde{q}_j}{\partial x_j} + \frac{\partial(\tilde{\sigma}_{ij}\tilde{u}_i)}{\partial x_j} - \frac{\partial q_j^{sgs}}{\partial x_j} \cdot \frac{1}{(\gamma - 1)M_f^2}. \quad (16)$$

In Eq. (15), $\tilde{\sigma}_{ij}$ is the viscous stress tensor based on the filtered quantities, while τ_{ij}^{sgs} is the sub-grid scale stress tensor. The last term $(\tilde{\sigma}_{ij} - \tau_{ij}^{sgs})$ arises due to the nonlinearity of the viscous stresses. In Eq. (16), q_j^{sgs} is the sub-grid term due to nonlinearity of the advective energy flux. The modeling of the sub-grid terms is discussed in Section IV A.

III. Numerical Method

In this section we provide a brief description of the numerical method employed for the simulation. Complete description of the method could be found in Refs.^{11,12}

A. Nodal element

The nodal approximation basis requires construction of a multivariate Lagrangian interpolant within a tetrahedron. We begin by considering a smooth and invertible mapping function $\Psi : D \rightarrow I$ that maps any straight face tetrahedral element D to the standard tetrahedron I . Thus any $\mathbf{x} \in D$ is mapped to $\boldsymbol{\xi} \in I$. Since we consider only straight face tetrahedron, the transformation jacobian and metric of the transformation is constant. This allows us to develop the numerical scheme on the standard tetrahedron I and apply it to the physical element D by linear rescaling. Next we describe the construction of Lagrange interpolation function within the standard tetrahedron I . The natural polynomial space for the approximation functions defined on the tetrahedron is ,

$$P_n^3 = \text{span}\{\xi^i \eta^j \zeta^k; i, j, k \geq 0; i + j + k \leq n\}, \quad (17)$$

where n is the order of the polynomial. The dimension of the above approximation space is,

$$\dim P_n^3 = N_n^3 = \frac{(n+1)(n+2)(n+3)}{6}, \quad (18)$$

which is also the size of the n th-order generalized Pascal triangle.¹³ In-order to derive a Lagrangian interpolation basis we introduce the nodal set, $\Pi_n^3 = (\boldsymbol{\xi}_0, \dots, \boldsymbol{\xi}_N)$ where $\boldsymbol{\xi}_\alpha$ are the node points within the tetrahedron I and $N = N_n^3 - 1$. The derivation of the Lagrangian basis relies on the introduction of complete polynomial basis, $p_\alpha(\boldsymbol{\xi}) \in P_n^3$, such that any smooth function $f(\boldsymbol{\xi})$ defined in I would have the interpolation property,

$$\Upsilon_n^3 f(\boldsymbol{\xi}_\alpha) = f(\boldsymbol{\xi}_\alpha) = \sum_{\beta=0}^N a_\beta p_\beta(\boldsymbol{\xi}_\alpha), \quad \forall \alpha \in [0, \dots, N] \quad (19)$$

which can also be written in the matrix form,

$$\mathbf{f} = \mathbf{V} \mathbf{a}, \quad V_{\alpha\beta} = p_\beta(\boldsymbol{\xi}_\alpha), \quad (20)$$

where V is the Vandermonde matrix. We now define a Lagrangian basis as,

$$\Upsilon_n^3 f(\boldsymbol{\xi}) = f(\boldsymbol{\xi}) = \sum_{\alpha=0}^N f(\boldsymbol{\xi}_\alpha) L_\alpha(\boldsymbol{\xi}), \quad (21)$$

where the Lagrange polynomial has the cardinal property, $L_\alpha(\boldsymbol{\xi}_\beta) = \delta_{\alpha\beta}$. The polynomials L_α are recovered by solving the interpolation problem,

$$p_\beta(\boldsymbol{\xi}) = \sum_{\alpha=0}^N p_\beta(\boldsymbol{\xi}_\alpha) L_\alpha(\boldsymbol{\xi}), \quad \forall \beta \in [0, \dots, N], \quad (22)$$

$$\mathbf{V}^T \mathbf{L} = \mathbf{p}.$$

The success of the above method depends heavily on the choice of the polynomial basis $p_\beta(\boldsymbol{\xi})$ and the multidimensional nodal set Π_n^3 . The polynomial basis used in this work is obtained from the classical Jacobi

polynomial (see Hesthaven¹³). Nodal set distribution computed by Hesthaven¹³ is employed in this work. This combination guarantees a well conditioned Vandermonde matrix and consequently efficient computation of the Lagrange polynomials.

B. Discretization of the governing equations

Having established a suitable high-order approximation basis within the tetrahedron we now proceed to briefly describe the basics of the discretization and solution of the governing partial differential equations. The computational domain (Ω) is represented by union of non-overlapping tetrahedral elements D_k . Thus

$$\Omega = \sum D_k. \quad (23)$$

We approximate the state vector in each element as

$$\mathbf{q}(\mathbf{x}, t) \approx \mathbf{q}_N(\mathbf{x}, t) = \sum_{\alpha=0}^N \mathbf{q}_\alpha(t) L_\alpha(\mathbf{x}), \quad \forall \mathbf{x} \in D_k, \quad (24)$$

where $\mathbf{q}_\alpha(t) = \mathbf{q}(\mathbf{x}_\alpha, t)$ and $N + 1$ is the total number of node points within the tetrahedron. Similar approximation is considered for the flux vectors \mathbf{F} ,

$$\mathbf{F}(\mathbf{x}, t) \approx \mathbf{F}_N(\mathbf{x}, t) = \sum_{\alpha=0}^N \mathbf{F}_\alpha(t) L_\alpha(\mathbf{x}), \quad \forall \mathbf{x} \in D_k, \quad (25)$$

where $\mathbf{F}_\alpha(t) = \mathbf{F}(\mathbf{x}_\alpha, t)$. With the polynomial approximation in place, we now put the equation in the strong form of the discontinuous Galerkin formulation,

$$\int_{D_k} \left(\frac{\partial \mathbf{q}_N}{\partial t} + \nabla \cdot \mathbf{F}_N \right) L_\alpha(\mathbf{x}) d\mathbf{x} = \oint_{\partial D_k} L_\alpha(\mathbf{x}) \mathbf{n} \cdot (\mathbf{F}_N - \mathbf{F}^*) d\mathbf{x}. \quad (26)$$

The numerical flux \mathbf{F}^* is used to enforce elemental coupling or in other words to pass information between elements. Substitution of the polynomial approximations in the above equation leads to local operators,

$$\widehat{M}_{\alpha\beta} = \int_{D_k} L_\beta L_\alpha d\mathbf{x}, \quad \widehat{S}_{\alpha\beta} = \int_{D_k} \nabla L_\beta L_\alpha d\mathbf{x}, \quad \widehat{F}_{\alpha\beta} = \oint_{\partial D_k} \nabla L_\beta L_\alpha d\mathbf{x}. \quad (27)$$

The use of the above operators transforms the equation into

$$\widehat{M} \frac{d\mathbf{q}}{dt} + \widehat{S} \cdot \mathbf{F} = \widehat{F} \mathbf{n} \cdot [\mathbf{F}(\mathbf{q}^-) - \mathbf{F}^*(\mathbf{q}^+, \mathbf{q}^-)]. \quad (28)$$

In the above form \mathbf{q} denotes the $4N$ vector coefficients for \mathbf{q}_N , and similarly for \mathbf{F} and \mathbf{F}^* . The superscript ‘-’ refers to the values local to the element whereas ‘+’ refers to the values from the neighboring elements. We finally complete our formulation with a prescription for the numerical flux \mathbf{F}^* . In this work a Lax-Friedrichs flux is chosen to represent the numerical flux,

$$\mathbf{n} \cdot [\mathbf{F} - \mathbf{F}^*] = \mathbf{n} \cdot [\mathbf{F}^- - \mathbf{F}^+ + |\lambda|(\mathbf{q}^+ - \mathbf{q}^-)]. \quad (29)$$

where $|\lambda|$ is the largest eigenvalue of the linearised system of equations. It is taken to be the global maximum of $|(u^2 + v^2 + w^2)^{1/2} + c_{air}|$.

IV. Closure of LES Equations

In this section we describe the methodology for closing the governing equations for LES.

A. Sub-grid scale model

The filtered Navier-Stokes equations are unclosed because of the presence of the sub-grid terms, which need to be modeled. These terms physically represent the effect of the unresolved (sub-grid) scales on the resolved scales. Let us consider the modeling of the unclosed terms in the momentum equation first.

The term $(\bar{\sigma}_{ij} - \tilde{\sigma}_{ij})$ is neglected following Refs.^{16,17} The sub-grid term $\tau_{ij}^{sgs} = \bar{\rho}(\widetilde{u_i u_j} - \tilde{u}_i \tilde{u}_j)$ is modeled using the modification of the Germano model¹⁸ for compressible flows (given by Moin et al.¹⁹). The expression for τ_{ij}^{sgs} is accordingly given as

$$\tau_{ij}^{sgs} = -2C_s \bar{\Delta}^2 \bar{\rho} |\tilde{S}| \left(\tilde{S}_{ij} - \frac{1}{3} \tilde{S}_{mm} \delta_{ij} \right) + \frac{1}{3} \tau_{kk}^{sgs} \delta_{ij}. \quad (30)$$

The trace of the sub-grid stress tensor τ_{kk}^{sgs} cannot be included in the modified pressure in compressible flow, and thus has to be modeled separately. Different models of τ_{kk}^{sgs} have been proposed (see Refs.^{20,21}). However studies by Squires²² demonstrated that there is no difference in the LES results of compressible isotropic turbulence at low Mach number when τ_{kk}^{sgs} is neglected. Vreman et al.²³ confirmed the above findings with their simulation of 3D compressible mixing layers at a mean convective Mach number of 0.2. In *a priori* test, the SGS model that neglects τ_{kk}^{sgs} was found to be in better agreement with DNS results. Moreover, simulations conducted with a dynamic model for τ_{kk}^{sgs} were often unstable for the cases studied. Thus we conclude that for low Mach number LES, neglecting the trace of sub-grid stress tensor will not introduce large errors and in some cases might be beneficial. As a result we neglect the term in this work. The details of the dynamic procedure to obtain the estimate for $C_s \bar{\Delta}^2$ are provided in Section B. The sub-grid term in the energy equation (q_j^{sgs}) due to nonlinearity of the advective fluxes is given as (for complete derivation see Ref.²),

$$q_j^{sgs} = \bar{\rho} \left(\widetilde{T u_j} - \tilde{T} \tilde{u}_j \right). \quad (31)$$

This term is modeled using the eddy-viscosity hypothesis and a turbulent Prandtl number.¹⁹ Accordingly the modeled expression is,

$$q_j^{sgs} = \frac{\bar{\rho} C_s \bar{\Delta}^2 |\tilde{S}|}{Pr_t} \frac{\partial \tilde{T}}{\partial x_j}. \quad (32)$$

The turbulent Prandtl number Pr_t is evaluated using the dynamic procedure (see Section B). The sub-grid term due the nonlinearity of the viscous work term ($u_i \sigma_{ij}$) is neglected following the work of Vreman et al.¹⁶

B. Dynamic procedure

The dynamic model¹⁸ is based on the supposition that in the inertial range of the turbulence energy spectrum, the physics is statistically self similar at different length scales. Therefore, same functional form for the sub-grid quantities can be assumed at the grid length scale $\bar{\Delta}$, representative of the computational mesh, and at a larger test filter length scale $\hat{\Delta}$. The application of the test filter to the grid filtered Navier-Stokes (Eq. (15)) leads to a residual stress at the test filter level,

$$T_{ij} = \widehat{\rho u_i u_j} - \frac{\widehat{\rho u_i \rho u_j}}{\widehat{\rho}}. \quad (33)$$

Similarly applying the test filter to the residual stresses at the grid filter level (τ_{ij}^{sgs}) gives,

$$\widehat{\tau}_{ij}^{sgs} = \widehat{\rho u_i u_j} - \frac{\widehat{\rho u_i \rho u_j}}{\widehat{\rho}}. \quad (34)$$

The difference between Eq. (33) and Eq. (34) leads to the Germano's identity,

$$L_{ij} = T_{ij} - \widehat{\tau}_{ij}^{sgs} = \widehat{\rho \tilde{u}_i \tilde{u}_j} - \frac{\widehat{\rho \tilde{u}_i \rho \tilde{u}_j}}{\widehat{\rho}}. \quad (35)$$

Assuming that same functional form (Smagorinsky model) could be used for the residual stresses at both levels, we have the modeled forms as,

$$T_{ij} = -2C_s \widehat{\Delta}^2 \widehat{\rho} |\widehat{S}| \left(\widehat{S}_{ij} - \frac{1}{3} \widehat{S}_{mm} \delta_{ij} \right) + \frac{1}{3} T_{kk} \delta_{ij}, \quad (36)$$

$$\tau_{ij}^{sgs} = -2C_s \overline{\Delta}^2 \overline{\rho} |\widetilde{S}| \left(\widetilde{S}_{ij} - \frac{1}{3} \widetilde{S}_{mm} \delta_{ij} \right) + \frac{1}{3} \tau_{kk}^{sgs} \delta_{ij}. \quad (37)$$

Now we define M_{ij} , as

$$M_{ij} = 2\overline{\rho} |\widetilde{S}| \left(\widetilde{S}_{ij} - \frac{1}{3} \widetilde{S}_{mm} \delta_{ij} \right) - 2 \frac{\widehat{\Delta}^2}{\overline{\Delta}^2} \widehat{\rho} |\widehat{S}| \left(\widehat{S}_{ij} - \frac{1}{3} \widehat{S}_{mm} \delta_{ij} \right), \quad (38)$$

where typically $\frac{\widehat{\Delta}^2}{\overline{\Delta}^2} = 2$ is assumed. Therefore, the modeled form of L_{ij} is given by

$$L_{ij} = C_s \overline{\Delta}^2 M_{ij} - \frac{1}{3} \tau_{kk}^{sgs} \delta_{ij} + \frac{1}{3} T_{kk} \delta_{ij}. \quad (39)$$

Here we neglect both τ_{kk}^{sgs} and T_{kk} . Finally, using Lily's²⁴ least square minimization procedure we obtain,

$$C_s \overline{\Delta}^2 = \frac{L_{ij} M_{ij}}{M_{kl} M_{kl}}. \quad (40)$$

This procedure gives a local time dependent estimate of $C_s \overline{\Delta}^2$, which is updated at every time step in the computation. It is worthwhile to note that the above procedure computes the Smagorinsky length scale $C_s \overline{\Delta}^2$ directly without the need to specify the grid filter width $\overline{\Delta}$. This is advantageous in the current context considering that for unstructured grids it is generally difficult to provide an expression for the filter width $\overline{\Delta}$.

C. Element level filtering

The dynamic procedure involves explicit application of the filter (test filter) on the grid filtered quantities. In this work we employ a smooth element based filtering approach following Blackburn and Schmidt.⁷ Since our polynomial basis functions p_β form a hierarchical set, implying that they have progressively higher spatial frequencies, we can apply a low pass filter in the spectral space to remove the high frequency modes (small scales). The solution of the discretized equations leads to nodal values of the state vector (see Section III B). Therefore, in-order to apply the filtering in spectral space we need to transform the solution from the nodal representation (q) to modal (q^*) representation. This is implemented by discrete polynomial transform. If p_β are the polynomial basis functions then the nodal values of any smooth function $q(\mathbf{x})$ could be represented by the spectral expansion,

$$q(\mathbf{x}_\alpha) = \sum q_\beta^* p_\beta(\mathbf{x}_\alpha), \quad (41)$$

as in Eq. (19). In matrix vector form this is represented as

$$\mathbf{q} = \mathbf{V} \mathbf{q}^*, \quad (42)$$

where \mathbf{V} is the Vandermonde matrix defined in Eq. (20). The spectral coefficients (\mathbf{q}^*) are recovered by taking the inverse of \mathbf{V} ,

$$\mathbf{q}^* = \mathbf{V}^{-1} \mathbf{q}. \quad (43)$$

Now the spectral filter could be applied in the space of the coefficients \mathbf{q}^* . Let us define a filter vector l_k and filter diagonal $\mathbf{L} = \text{diag}(l_0, \dots, l_N)$. The filtered modal values $\overline{\mathbf{q}}^*$ are produced by the matrix operation,

$$\overline{\mathbf{q}}^* = \mathbf{L} \mathbf{V}^{-1} \mathbf{q}, \quad (44)$$

from which the filtered nodal values could be recovered as,

$$\overline{\mathbf{q}} = \mathbf{V} \mathbf{L} \mathbf{V}^{-1} \mathbf{q} = \mathbf{F} \mathbf{q}. \quad (45)$$

The filter weights l_k can be chosen in an appropriate manner. For example, l_k could be a spectral top-hat filter, or a set that is smooth in spectral space, such as exponential filter²⁵ or Boyd-Vandeven coefficients.⁸

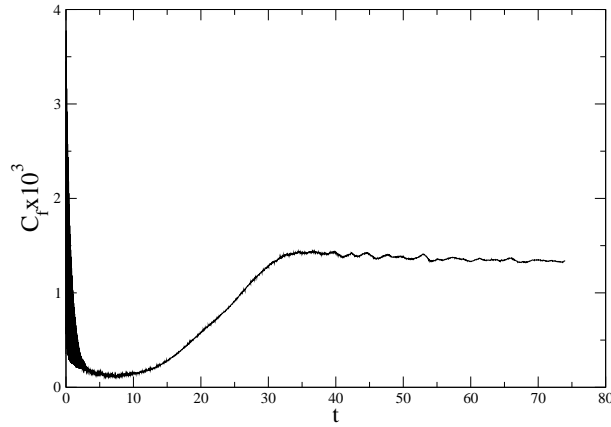


Figure 1. Evolution of wall shear stress for 2D Poiseuille flow (DNS).

V. Results and Discussion

Real turbulence is always three-dimensional. Transition to turbulence for plane parallel (uni-directional) shear flows is a very complicated phenomenon, encompassing both linear and nonlinear instability mechanisms. At sufficiently high Reynolds number, plane Poiseuille flow becomes unstable due to the growth of the 2D waves, known as Tollmien-Schlichting (TS) waves. In the absence of any short-wave 3D disturbances, the TS waves equilibrate at some finite amplitude. The presence of 3D perturbations will lead to complete breakdown of these waves and the flow degenerates into fully developed turbulence.²⁶ In a real transition situation, there may not be any distinct 2D and 3D phases present. In other words 3D disturbances do not necessarily wait till 2D equilibrium is established before entering into the flow dynamics. Nevertheless, attempts have been made to isolate the role of 2D structures in transition to turbulence through 2D numerical simulations (e.g. Ref.²⁷). Since the main objective of the present work is to validate the code for turbulent channel flow, we start by simulating 2D Poiseuille flow at high Reynolds number to verify the ability of our method to capture the 2D TS waves. The next phase would be to perform 3D simulations and validate the code against existing data in the fully turbulent regime of the flow. It must again be pointed out that no attempt is being made here to study the nature of complete transition to turbulence (which would heavily depend on the presence of 3D modes), but only to investigate the ability of the numerical method to capture the initial transition phenomena which are predominantly 2D.

We perform both DNS and LES for the flow. For the DNS case we use a mesh with 8,958 elements (non-uniform in the wall normal direction) and polynomial order $n = 5$. Since the flow is periodic in the streamwise direction, a time dependent body force is added to the momentum equation to drive the flow. It has been shown by Lenormand et. al.,²⁸ that specifying a constant source term leads to a mass flux that is time dependent. This makes analysis at constant Reynolds number impossible. Therefore, in order to maintain a constant mass flux, the source term needs to be time dependent. We employ the algorithm presented in Ref.,²⁸ to calculate the time dependent forcing term. From the linear stability theory, the critical Reynolds number for the 2D Poiseuille flow is $Re_{cr} = 5,772$.²⁹ The geometry of the channel is chosen such as $L_x = 7$ and $L_y = 1$. The flow is simulated at Reynolds number of $Re = 10,000$ based on channel half width and average velocity. The Mach number is chosen to be $Ma = 0.1$ so that the effects of compressibility are small.

Figure 1 shows the time evolution of skin friction coefficient for the DNS case. We observe that the initial random perturbations are damped out around $t = 5$ and only the unstable TS modes start to grow thereafter. At about $t = 35$ they eventually equilibrate due to the absence of any three-dimensional disturbances. The instantaneous plot of streamwise momentum flux (Figure 2) at three different times, shows the presence of the TS waves. The peaks correspond to high velocity fluctuations while the valleys represent low fluctuations.

Next, we investigate the effect of the sub-grid model with two different filters: sharp spectral (top hat) filter and smooth (exponential filter) on the same flow. A common concern with spectral element filtering is that the filtering does not preserve the inter-element continuity and boundary conditions (C^0 continuity). However, that is not an issue for an inherently discontinuous method used here. Moreover, filtering is

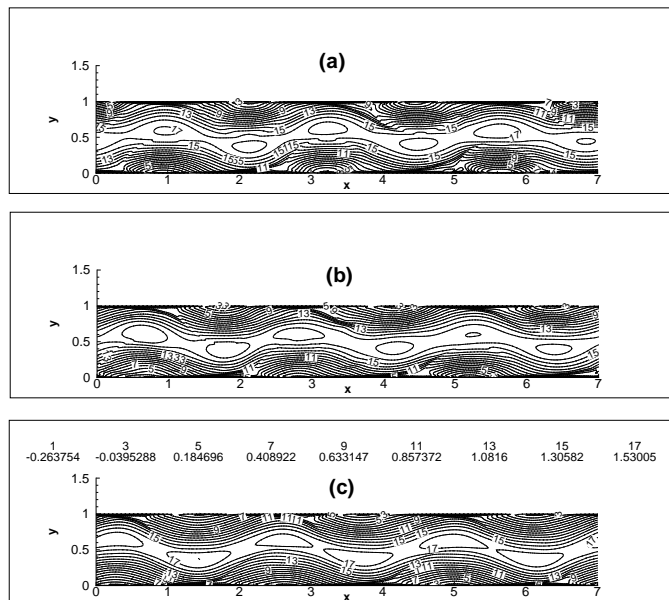


Figure 2. Streamwise momentum flux for 2D Poiseuille flow from DNS: (a) $t=40$ (b) $t=60$ (c) $t=80$.

applied to the intermediate fields only to construct the eddy viscosity estimate. Figure 3 shows streamwise momentum contours for LES cases for two different filter types. A total of 4,144 elements and $n = 5$ were used for the cases. Comparison with DNS case indicates that the top hat filter result agrees better. Finally, we compare statistics from the DNS and LES (with top hat filter) runs. Figure 4 shows the Favre averaged axial velocity profiles, where we observe excellent match. The average normal velocity was found to be non-zero due to the algorithm employed to calculate the time dependent source term in the axial momentum equation, which is not fully mass conserving. Increasing the order of the polynomial reduces the discrepancy in the normal velocity. Figure 5 shows the velocity fluctuations (again Favre averaged) for the two cases, normalized by the friction velocity. The LES case over-predicts both U_{rms} (maximum difference near the wall) and V_{rms} (maximum difference at the center of the channel).

VI. Conclusions

A high-order discontinuous Galerkin method on unstructured grids has been proposed for large-eddy simulation in complex geometries. The basics of the numerical scheme and sub-grid modeling approach have been discussed. Transition phenomenon in two-dimensional Poiseuille flow at high Reynolds number is investigated. The numerical method is able to capture the unsteady features which are characteristic of high Reynolds number. Work is currently underway to develop the 3D code and validate it against DNS and experimental database for fully turbulent plane channel flow.

Acknowledgments

The support for this work was provided by the U.S. Office of Naval Research with Dr. G.D. Roy as the Program Officer. The authors would like to thank Dr. Paul Fischer for useful comments on the stability analysis of Poiseuille flow.

References

- ¹Lele, S.K., A compact finite difference schemes with spectral like resolution, *Journal of Computational Physics*, 103, 16, 1992.
- ²Santhanam, S., Lele, S.K., and Ferziger, J.H., A robust high-order compact method for large-eddy simulation, *Journal of Computational Physics*, 191, 392-419, 2003.
- ³Jansen, K.E., A stabilized finite element method for computing turbulence, *Comput. Methods. Appl. Mech. Engrg*, 174,

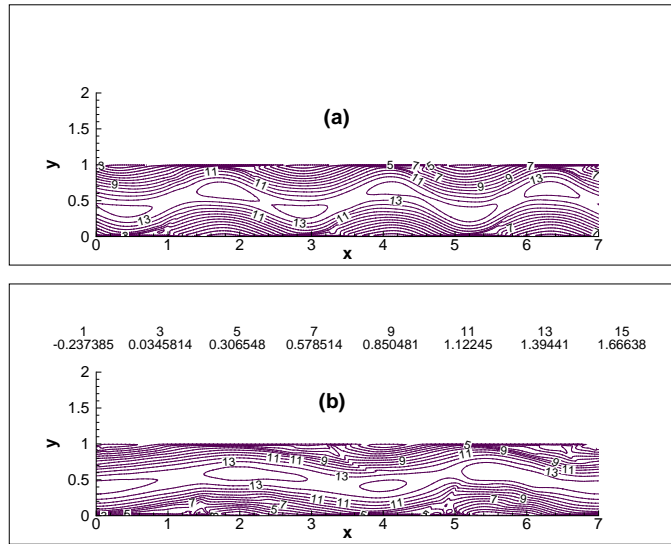


Figure 3. Streamwise momentum flux for 2D Poiseuille flow from LES. (a) Top hat filter, (b) exponential filter.

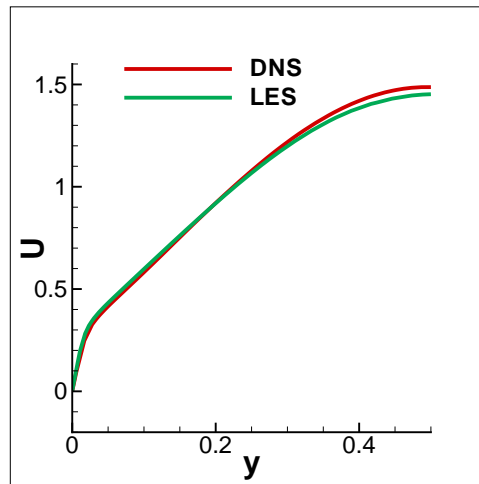


Figure 4. Favre averaged axial velocity for DNS and LES.

299-317, 1999.

⁴Bui, T.T., A parallel, finite volume algorithm for large-eddy simulation of turbulent flows, *Computer and Fluids*, 29, 877-915, 2000.

⁵Jacobs, G.B., Kopriva, D.A., and Mashayek, F., Validation study of multidomain spectral element code for simulation of turbulent flows, *AIAA J.*, 43(6), 1256-1264, 2004.

⁶Ghosal, S., An analysis of numerical errors in large-eddy simulations of turbulence, *Journal of Comput. Phys.*, 125, 187-206, 1996.

⁷Blackburn, H.M., and Schmidt, S., Spectral element filtering techniques for large eddy simulation with dynamic estimation, *Journal of Computational Physics*, 186, 610-629, 2003.

⁸Levin, J.G., Iskandarani, M., and Haidvogel, D.B., A spectral filtering procedure for eddy-resolving simulations with a spectral element ocean model, *Journal of Computational Physics*, 137, 130-154, 1997.

⁹Karamanos, G.S., Large eddy simulation using unstructured spectral/hp finite elements, *PhD Thesis, Imperial College of Science and Technology*, 1999.

¹⁰Karamanos, G.S., and Karniadakis, G.E., A spectral vanishing viscosity method of large-eddy simulations, *Journal of Computational Physics*, 163, 22-50, 2000.

¹¹Hesthaven, J.S., and Gottlieb, D., Stable spectral methods for conservation laws on triangles with unstructured grids, *Comput. Methods Appl. Engrg*, 175, 361-381, 1999.

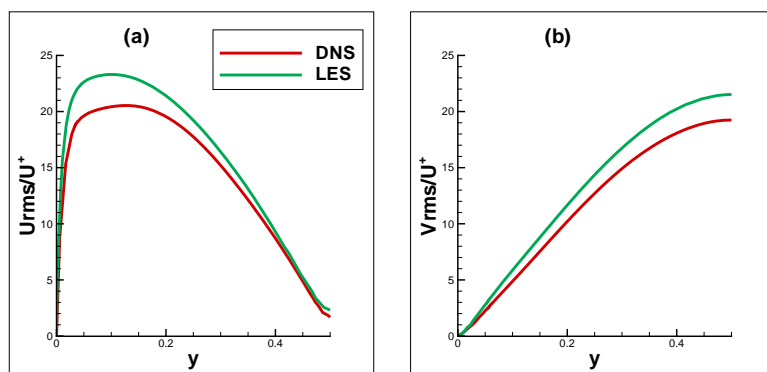


Figure 5. Normalized velocity fluctuations in (a) streamwise and (b) cross-stream directions.

¹²Hesthaven, J.S, and Teng, C.H., Stable spectral methods on tetrahedral elements, *SIAM J. SCI. COMPUT.*, 21(6), 2352-2380, 2000.

¹³Hesthaven, J.S, From electrostatics to almost optimal nodal sets for polynomial interpolation in a simplex, *SIAM J. Numer. Anal.*, 35, 655-676, 1998.

¹⁴Sagaut, P., Large Eddy Simulation for Incompressible Flow, *Springer*, 2000.

¹⁵Favre, A., Equations statistiques aux fluctuations turbulentes dans les écoulements compressibles: cas des vitesses et des temperature, *C. R. Acad. Sci. Paris.*, 273, 1087, 1971.

¹⁶Vreman, B., Guerts, H., and Kuerten, H., Subgrid-modeling in LES of compressible flow, *Appl. Sci. Res.*, 54, 191, 1985.

¹⁷Vreman, B., Guerts, H., and Kuerten, H., A priori tests of large eddy simulation of compressible mixing layer, *J. Eng. Math.*, 29, 299-327, 1995.

¹⁸Germano, M., Piomelli, U., Moin, P., and Cabot, W.H., A dynamic subgrid scale eddy viscosity model, *Phys. Fluids A* 3, 7, 1760-1765, 1991.

¹⁹Moin, P., Squires, K., Cabot, W., and Lee, S., A dynamic subgrid model for compressible turbulence and scalar transport, *Phys. Fluids A* 3, 11, 2746-2757, 1991.

²⁰Yoshizawa, A., Statistical theory for compressible turbulent shear flows, with the application to subgrid modeling, *Physics of Fluids A*, 29, 2152-2164, 1986.

²¹Erlebacher, G., Hussaini, M.Y., Speziale, C.G., and Zang, T.A., Toward the large eddy simulation of compressible turbulent flows, *Journal of Fluid Mechanics*, 238, 155-185, 1992.

²²Squires, K.D., Dynamic subgrid scale modeling of compressible turbulence, *Annual Research Brief, Stanford University*, 1991.

²³Vreman, A.W., Guerts, B.J., and Kuerten, JGM, Subgrid modeling of LES of compressible flow, *Direct and large eddy simulation I, Kluwer academic publisher, Netherlands*, 1994.

²⁴Lily, D.K., A proposed modification of the Germano subgrid-scale closure method, *Phys. Fluids A* 4, 3, 633-635, 1992.

²⁵Gotlieb, D., and Hesthaven, J.S., Spectral methods for hyperbolic problems, *J. Comput. and Appl. Math.*, 128, 83-131, 2000.

²⁶Orszag, S.A., and Bayly, B.J., Instability mechanisms in shear-flow transition, *Ann. Rev. Fluid Mech.*, 20, 359-391, 1988.

²⁷Jiménez, J., Bifurcation and bursting in two-dimensional Poiseuille flow, *Phys. Fluids*, 30, 3644-3646, 1987.

²⁸Lenormand, E., Sagaut, P., and Ta Phuoc, T., Large eddy simulation of subsonic and supersonic channel flow at moderate Reynolds number, *Int. J. Numer. Meth. Fluids*, 32, 369-406, 2000.

²⁹Drazin, P.G., and Reid, W.H., *Hydrodynamic Stability, Cambridge University Press*, 1981.